



A numerical and experimental study on the obstacle collision avoidance system using a 2D LiDAR sensor for an autonomous surface vehicle

Ji-Soo Kim, Dong-Hun Lee, Dae-Woong Kim, Hyeri Park, Kwang-Jun Paik, Sanghyun Kim*

Department of Naval Architecture and Ocean Engineering, Inha University, Incheon, South Korea

ARTICLE INFO

Keywords:

Autonomous surface vehicle (ASV)
Collision avoidance
Decision making
Ship domain
Obstacle avoidance guidance
2D LiDAR sensor

ABSTRACT

In recent years, great efforts have been made to develop unmanned navigation systems for Autonomous Surface Vehicles (ASVs), while further improvements are still required for ASVs operating around obstacles. In this circumstance, this paper presents an Obstacle Collision Avoidance Guidance (OCAG) using obstacle detection with a two-dimensional (2D) LiDAR sensor. After verifying the algorithm of the OCAG in a numerical manoeuvring simulation, the OCAS was embedded in a physical model of a Catamaran-type ASV with a 2D LiDAR sensor. When the ASV sails along with a predefined global path, the LiDAR sensor detects the obstacles, the collision-avoidance actions are determined based on multiple factors including the motion and orientation information of the vehicle, the measured distance and direction information of the obstacles, as well as the types of the obstacles. The proposed OCAG showed good collision-avoidance performances with different obstacle types along the path.

1. Introductions

As interest in unmanned systems has been growing, there has been active research on autonomous navigation systems. In these circumstances, the reliability of unmanned systems has been improved rapidly and commercialized in various industries in recent years. This trend has also been observed in the shipbuilding industry, and efforts are being made to provide a fully autonomous ship through autonomous navigation systems or support for navigation through auxiliary systems for sailors (Kim et al., 2020). Unlike autonomous ground vehicles, autonomous surface vehicles (ASV) operating in the ocean are relatively slow to respond to obstacles. For this reason, a proactive Obstacle Collision Avoidance Guidance (OCAG) is required which considers various factors, such as the distance, bearing, and speed of other vessels, floats (such as breakwaters and buoys), reefs, etc.

The key components of an autonomous navigation system are Navigation, Guidance and Control (NGC). The Navigation of NGC (ABS, 2021), which refers to the sensing and monitoring parts, is a critical component of an autonomous navigation system for proper obstacle detection and measurement of ship-movement information for an ASV (Campbell et al., 2012). The navigation system calculates the current states of the ASV (e.g. position, direction, and speed). The calculation is based on the past and current states and environmental loads (e.g.

current and wind speeds). Based on the information calculated by the navigation system, the guidance system continuously generates and updates optimal control commands for behaviors such as path following and obstacle avoidance (Woo and Kim, 2020). The control system is configured to perform the desired control command by determining the appropriate forces and moments (Liu et al., 2016).

This autonomous navigation system obtains accurate position information of the obstacles using sensors such as radar, LiDAR, and cameras (Ahn et al., 2012). It avoids collisions with obstacles through algorithm-based obstacle avoidance systems (Song et al., 2019). Recently, the use of LiDAR sensor has been the mainstream over the conventional radar systems (Wang et al., 2015), allowing accurate measurement of the distance and heading angle from nearby objects (Premeida and Nunes, 2005). However, due to the characteristics of LiDAR sensors, light can be dispersed to the surface of the sea, and signal noise from LiDAR can be caused by sea fog. Filtering techniques are being developed to minimize this noise and improve detection performance (Han et al., 2012).

Most ASVs are underactuated as they are not actuated in the sway axis for practical considerations (Dong et al., 2015). Therefore, many design techniques have been proposed for the control of an underactuated ASV. Harmouche et al. (2014) proposed a bound feedback controller for global tracking of ASVs, while Klinger et al. (2017) used a

* Corresponding author.

E-mail address: kimsh@inha.ac.kr (S. Kim).

back-stepping controller to control a target vessel to solve the uncertain resistance and mass characteristics of ASVs.

In this study, new Obstacle Collision Avoidance Guidance (OCAG) and systems were developed and embedded in a Catamaran-type ASV with a two-dimensional (2D) LiDAR sensor. The collision avoidance performance of the OCAS was evaluated by a numerical manoeuvring simulation with various obstacle types before the system is embedded in the physical model of the ASV. Finally, the performance of the OCAG was assessed with the physical ASV model sailing around various obstacles.

The remainder of this paper is organized as follows. In Section 2, the model and system configuration of ASVs used in the experiment are described. In Section 3, the proposed obstacle avoidance guidances are explained considering the ship domain of the ASV. In Section 4, the guidances are validated through simulations and experiments. In Section 5, the conclusions of the research and further discussion are reviewed.

2. Model and system configuration of autonomous surface vehicle

2.1. ASV hydrodynamic model

The ASV coordinate system used in this study was modeled as in Fig. 1. In Fig. 1, the position of the ASV is represented by a 3-DOF motion $G = [x, y, \psi]$. It moves in the XY plane and rotates around the Z-axis. ψ is the heading angle of the ASV relative to the earth-fixed coordinate system.

In this work, the ASV is assumed to be a rigid body with horizontal motion, and the ASV's motion is represented as 3-DOF motion with motion surge, sway, and yaw on the horizontal plane to express the control equation. The 3-DOF dynamic model of the ASV can be denoted as (Yasukawa and Yoshimura, 2015):

$$\begin{aligned} m(\dot{u} - vr) &= X_H + X_P \\ m(\dot{v} + ur) &= Y_H \\ I_{zG}\dot{\psi} &= N_H + N_P \end{aligned} \quad (1)$$

In the above expression, X , Y , and N represent the force in the X and Y directions and the moment for the N axis. The notation \cdot represents the time derivative, and the subscripts H and P represent the hydrodynamic force on the hull and propeller, respectively. The linearized hydrodynamic coefficients of the hull are as follows:

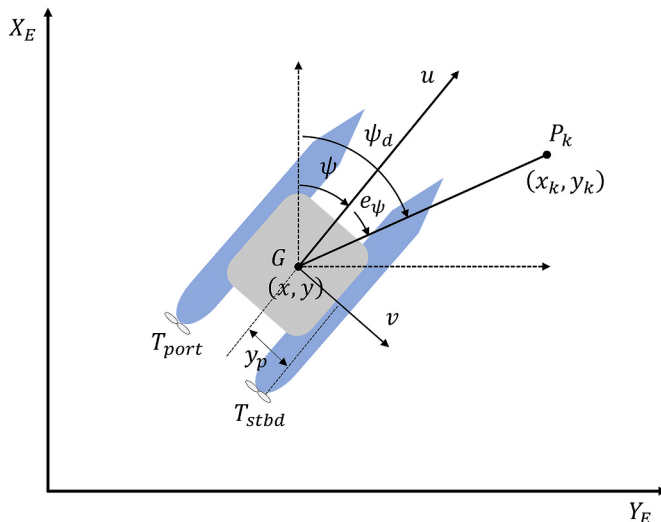


Fig. 1. Coordinate system of the ASV.

$$\begin{aligned} X_H &= -R_0 + X_{vv}v^2 \\ Y_H &= Y_{vv}v + Y_{rr}r + Y_{\dot{r}} \\ N_H &= N_{vv}v + N_{rr}r + N_{\dot{r}} \end{aligned} \quad (2)$$

Where X_{vv} , Y_{vv} , Y_{rr} , N_{vv} , N_{rr} are called hydrodynamic derivatives on maneuvering, and R_0 denotes the sum of the resistance. Note that the expression of the linearized function like Eq. (2) is not as sophisticated as the expression of the 1st and 3rd order polynomial function like Yasukawa (2015). However, the experimental environment in this paper is conducted in a place where no environmental loads are being applied, and the focus is on the development of collision avoidance. Therefore, the hydrodynamic model is used considering only the linear load and ignoring the environmental load. The external forces caused by the thruster are as follows. T_{port} and T_{stbd} denote the thrust of the port and starboard thruster, respectively, and y_p denotes the distance from the centreline of the ASV to the centreline of each side of the monohull.

$$\begin{aligned} X_P &= T_{Port} + T_{Stbd} \\ N_P &= (T_{Port} - T_{Stbd}) \times y_p \end{aligned} \quad (3)$$

2.2. Global path-following guidance of ASV

A conventional ASV control system is usually implemented with global path-following guidance, as shown in Fig. 2. Additionally, this paper focuses on the development of obstacle collision avoidance guidance. It is therefore used to follow a path before encountering obstacles using traditional simple but powerful methods. In this study, the steps of the ASV's global path-following guidance are as follows:

- Calculate the desired heading angle ψ_d between the waypoint P_k and x-axis direction X_E of earth-fixed coordinate system.
- Calculate the error angle e_ψ between the ASV's current heading angle ψ and desired heading angle ψ_d .
- Move ASV in the direction to reduce the error angle e_ψ .
- Calculate the distance $d(i)$ between the waypoint P_k and the current position $G(x_0, y_0)$.
- A criterion for switching to the next waypoint located at P_{k+1} is that the ASV must be within a circle of radius R_k from the current waypoint P_k . When $d(i)$ is within the predefined reachable criterion R_k , go to the next waypoint P_{k+1} .

The $P_k(x_k, y_k)$ of a waypoint and $G(x_0, y_0)$ of the ASV are the longitude and latitude coordinates shown above the geographic coordinate system. The values of longitude and latitude are not directly available for distance calculations, so they are converted to a projected coordinate system via Transverse Mercator (TM) projection.

$$\begin{aligned} x_d(i) &= x_k(i) - x_0(i) \\ y_d(i) &= y_k(i) - y_0(i) \\ d(i) &= \sqrt{x_d(i)^2 + y_d(i)^2} \end{aligned} \quad (4)$$

The distances x_d and y_d between the waypoint and the ASV, and the distance $d(i)$ from the ASV can be calculated using Eq. (4). In Fig. 2, ψ_d represents the desired heading angle for the ASV to proceed to the waypoint, and e_ψ is the error of the desired heading angle ψ_d and current heading angle ψ , which can be calculated using Eq. (5). For convenience, a clockwise angle is defined as a positive angle.

$$\begin{aligned} \psi_d(i) &= \text{atan}\left(\frac{y_d(i)}{x_d(i)}\right) \\ e_\psi(i) &= \psi_d(i) - \psi(i) \end{aligned} \quad (5)$$

R_k in Fig. 2 means the reference value for moving to the next waypoint, and when $d(i)$ is within $R_k = 2L_{pp}$, ASV moves to the next waypoint (Fossen, 2002).

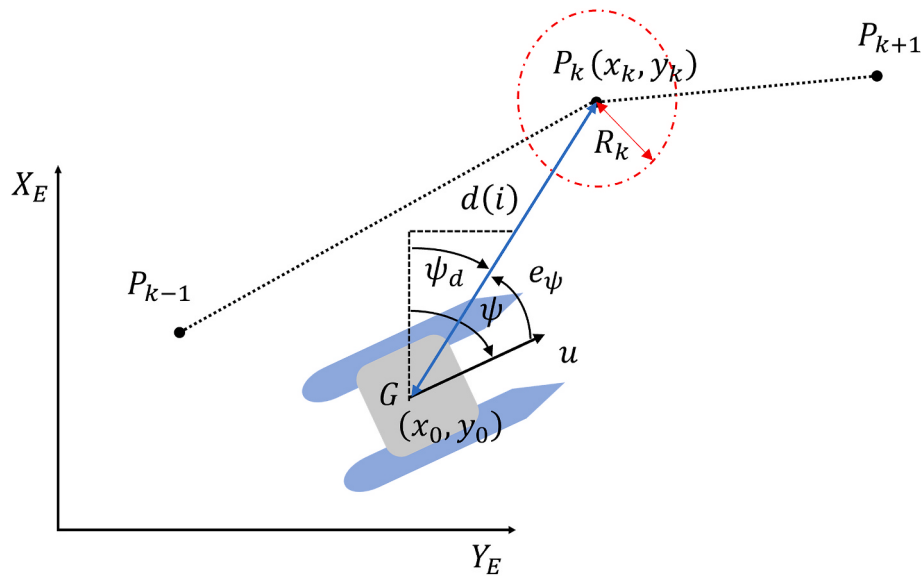


Fig. 2. Global path-following guidance.

2.3. Controller design of the autonomous surface vehicle

Usually, the manoeuvring control system of ships uses only the rudder for path following. However, the ASV used in this study adopted a steering system using the output difference of left and right thrust. The above method not only improves the turning performance at low speeds but also has the advantage of being able to finely control the ASV through reverse thrust. However, ASV is underactuated because the speed and steering must be controlled only through the thruster's output control without using a rudder. The controller is designed as shown in Fig. 3 to solve the underactuated ASV that requires speed and steering control at the same time through only thruster output control. At the same time, the output threshold considering the manufacturer's specifications is reflected in Fig. 3.

The speed controller reduces the error between the current speed and the design ship speed through a proportional derivative (PD) controller. It is also designed so that the sum of the RPM (revolutions per minute) of the PD controller and the nominal RPM at the design ship speed will be the result of the final speed controller. The ASV hydrodynamic model used in this study is linearized at the design speed U_d 1.1 m/s, and the P gain and D gain for speed control were also set to satisfy the design ship speed.

The steering controller determines the RPM for steering control

based on the desired heading angle ψ_d . Tolerance regions have been set for stable navigation, RPM for steering control is set to 0 when e_ψ is within $\pm 5^\circ$. Also, if e_ψ is greater than 5° , it means that a right turn is required, and a positive constant RPM is set for the left thruster, and a negative constant RPM is set for the right thruster. On the contrary, when e_ψ is less than -5° it means that a left turn is required, a negative constant RPM is set for the left thruster and a positive constant RPM is set for the right thruster.

Finally, the results of each of the speed controller and steering controller were added and used as the final RPM. The controller design as shown in Fig. 3 allows the ASV to control a stable heading angle and reach steady-state speed during movement.

2.4. System configuration of autonomous surface vehicle

The overall system structure of the ASV used in this study is shown in Fig. 4. It is divided into an onboard control system (ASV) and a remote control and monitoring station (ground). The entire software system was configured through a meta-operation system, the Robot Operating System (ROS). In addition, Python has been adopted as the programming language.

The onboard control system uses a Raspberry 4, a small embedded PC, as the main PC. The main PC sends and receives information from

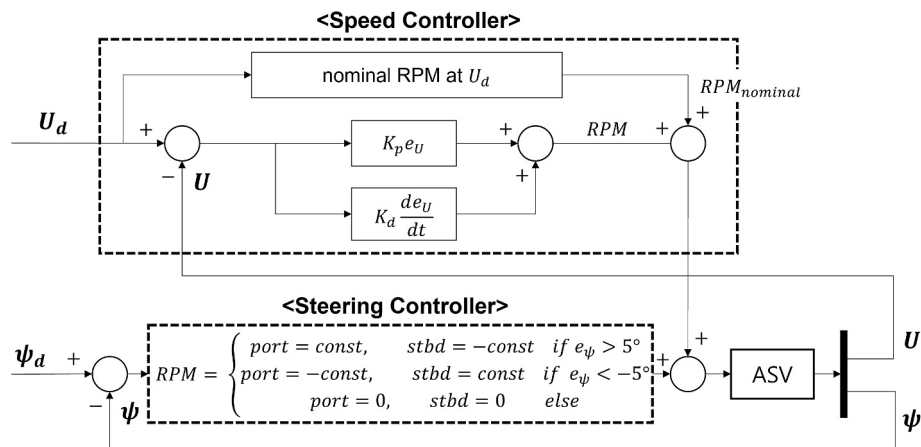


Fig. 3. Controller design: speed controller and steering controller.

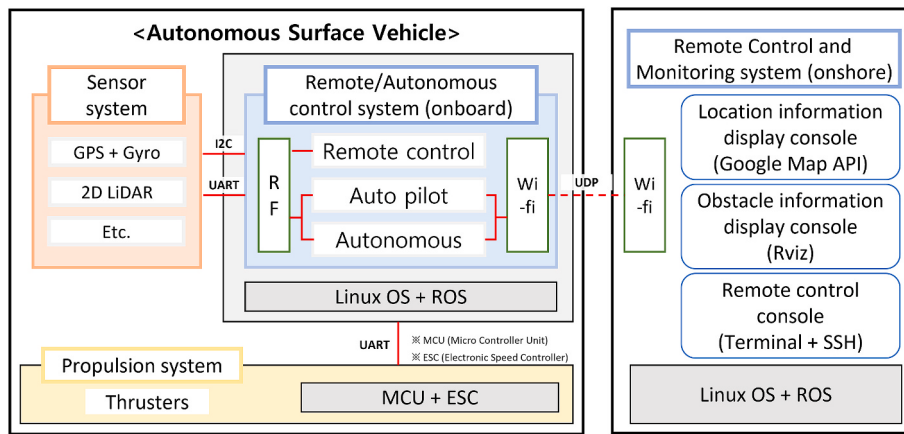


Fig. 4. System configuration diagram of the ASV.

LiDAR sensors to determine the direction, position, and distance of the obstacle, and GPS sensors to measure the current position of the ASV through UART communication. A U-Blox NEO M8N GPS sensor was also used in this work. It has an update cycle of 1 Hz and horizontal position accuracy of 2.5 m. Furthermore, the ASV's heading angle can be calculated based on the world coordinate system by using a smartphone's geomagnetic sensor measurements over TCP/IP communication with the main PC (Zhu et al., 2017). The microcontroller unit (MCU) is an Arduino. A pulse width modulation (PWM) signal is generated by the MCU and operates the thrusters via an electronic speed controller (ESC).

The remote control and monitoring station are configured to view information from the ASV in real-time over TCP/IP communication. The position information of the ASV is displayed on a map to monitor it, and the obstacle information obtained by the 2D LiDAR of the ASV is visualized using a 3D visualization tool called ROS RViz. The station can also provide control commands to manipulate the ASV.

Fig. 5 shows a diagram of the NGC system in the ASV. With the 2D LiDAR sensor, it is possible to estimate the obstacle position information in the direction of the ASV. In addition, geomagnetic sensors can be used to measure the heading angle of the current ASV, and GPS sensors can be utilized to estimate the current position information. The data measured by the geomagnetic sensor and the GPS sensor are used after removing noise through the complementary filter (Islam et al., 2017).

If an obstacle is not detected, the global path-following guidance defines the desired heading angle ψ_d so that the ASV aligns with the destination. This is done by comparing the current position of the ASV and the waypoint. While moving towards the set waypoint, the 2D LiDAR sensor continuously detects the front. If an obstacle is detected, the desired heading angle ψ_d is determined for the ASV avoidance action by static obstacle and line obstacle avoidance guidance based on the type, distance, and direction of the obstacle measured by the 2D LiDAR. In this work, the speed controller and steering controller were designed as shown in Fig. 3 to go to the destination and determine the final ship speed U and heading angle ψ of the ASV based on the ASV's design speed U_d and desired heading angle ψ_d . The above NGC system runs at every time step until ASV reaches its destination.

3. Collision avoidance guidance considering ship domain of the ASV

3.1. Ship domain and visible region of the ASV

The 2D LiDAR sensor used in this study enables high-precision measurement by continuously acquiring angle and distance information from obstacles through 360° rotation of the motor. So, the visible region of the LiDAR can cover the area with potential obstacles. The area

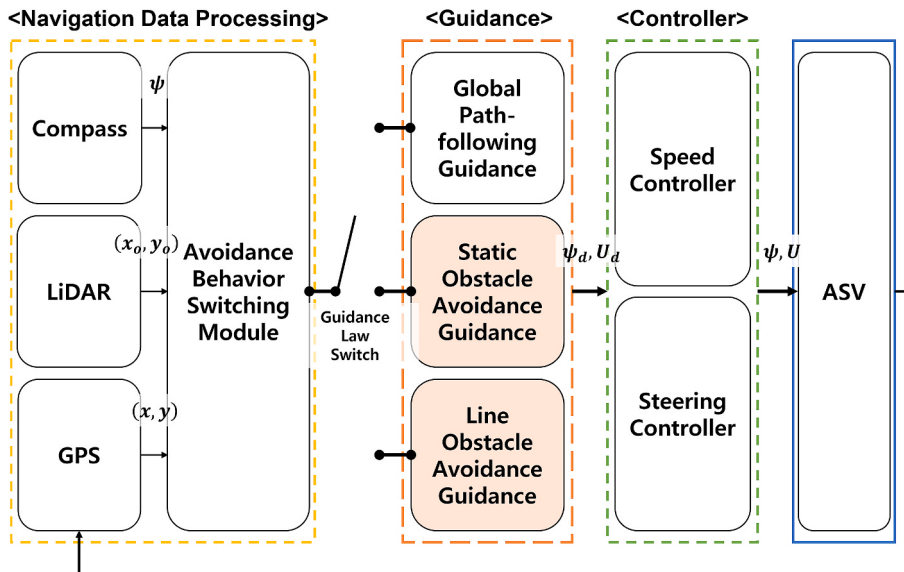


Fig. 5. Diagram of navigation, guidance, and control (NGC) system.

in which the ASV's LiDAR sensor can detect obstacles is shown in Fig. 6 (a).

An obstacle avoidance method needs to estimate when collision avoidance is performed, and a typical example is the ship domain. The ship domain refers to the two-dimensional area surrounding an own ship that a target ship should not enter. The collision avoidance behaviour begins when the target ship enters the ship domain (Fujii and Tanaka, 1971).

The obstacle collision avoidance system proposed in this research uses the ship domain to identify collision avoidance timing. In the ship domain, the safety distance to be secured was generalized by using the hull length among the principal dimensions of ASV. The ship domain of the ASV is shown in Fig. 6 (b). The size of the ship domain was defined through some experiments considering the design speed and inertial force of the ASV. In particular, the size was set in consideration of the main experimental environment. Since the main experimental environment has an aspect ratio of 3:1, it was designed to have a ship domain of 0.75 L in the transverse direction and 3 L in the longitudinal direction based on the ASV's center of gravity.

3.2. Static obstacle and line obstacle avoidance guidance

The collision avoidance action begins when an obstacle enters the ship domain and determines the action performed by the type of obstacle. Among the obstacles detected through the LiDAR sensor, the nearest obstacle was defined as a target to be avoided. Fig. 7 presents a collision-avoidance procedure when a static obstacle exists in the ASV's direction. The static OCAG calculates the angle $\theta_{intersection}$ that the obstacle can leave the ship domain when the obstacle enters the ship domain and uses the value as the desired heading angle ψ_d of the ASV.

Fig. 8 shows the line OCAG procedure when encountering obstacles such as walls. The previously defined static obstacle avoidance guidance is difficult to avoid collision with continuous straight (line) obstacles such as a wall because the risk of the collision remains simply by moving out of the ship domain. Therefore, when a line obstacle such as a wall is encountered, the angle $\theta_{intersection}$ between the line obstacle and the direction is calculated. When a line obstacle enters the ship domain of the ASV, the direction of movement is reversed to avoid the obstacle. However, at this time, additional angle compensation is provided for stable progress reversal and is used as the desired heading angle ψ_d of the ASV. The additional angle compensation has been defined through several experiments taking into account the design speed and size of the ASV.

3.3. OCAG algorithm considering the ship domain

The collision avoidance algorithm of the ASV used in the numerical simulation and experiment is shown in Fig. 9. First, the ASV moves along predefined global paths. When the ASV detects an obstacle on its way to its destination, the timing of the avoidance action is determined by an experimentally defined rectangular-shaped ship domain to avoid a collision. The collision avoidance action starts when the obstacle enters the ship domain, and the type of nearest obstacle determines which action to perform.

However, in the case of collision avoidance action, the safety of the ASV can be prioritized and may deviate from the predefined path. Therefore, when the ASV completes the collision-avoidance action and returns to the predefined path, it is designed to select the next waypoint if the relative angle between the direction of the ASV and the direction from the center of the ASV to the current waypoint is greater than 45° as shown in Fig. 10.

4. Collision avoidance simulation and experiment

4.1. Target ship of simulation and experiment

The Inha University Catamaran-type ASV (Fig. 11) was used in this study. It has a length of 1.445 m and a breadth of 0.767 m. The ASV's hydrodynamic model used was linearized at the design speed of 1.1 m/s. The thrusters are located near the ASV's center of gravity. The ASV generates propulsion by using thrusters installed in the centreline of each side of the monohull. In addition, since the thrusters are fixed to the hull, the control moment required for rotation can be generated by using the difference in the output of the left and right thrust. Table 1 shows the principal dimensions of the ASVs used in this study. The hydrodynamic force coefficients of the ASV for manoeuvring were derived from the process in Appendix A and are shown in Table 2.

4.2. Collision avoidance simulation results

As shown in Table 3, the main situation of collision avoidance simulation is divided into three categories: no obstacles, static obstacles, line obstacles (e.g. wall). The verifications through simulation are whether the collision-avoidance action is successful when detecting obstacles and whether it returns to a predefined global path.

- Case (i) The obstacle does not exist.
- Case (ii) Several static obstacles exist.
- Case (iii) A wall obstacle and some static obstacles exist.

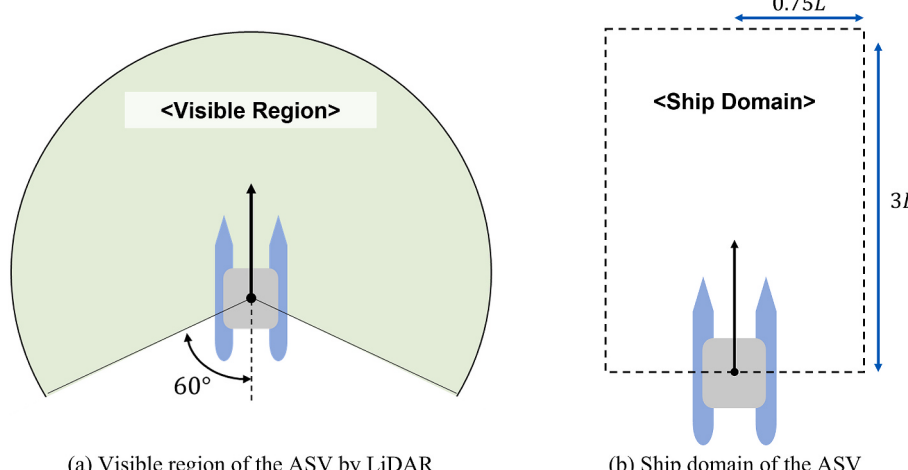


Fig. 6. Ship domain and obstacle detection region of the ASV for collision avoidance.

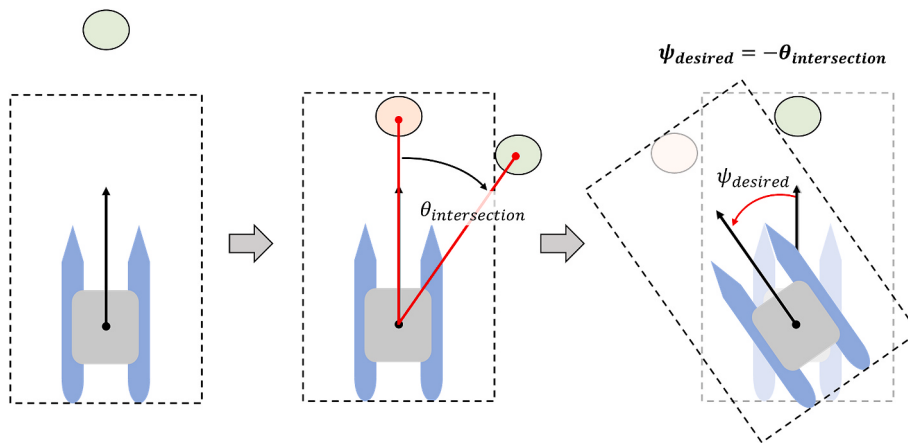


Fig. 7. Static OCAG

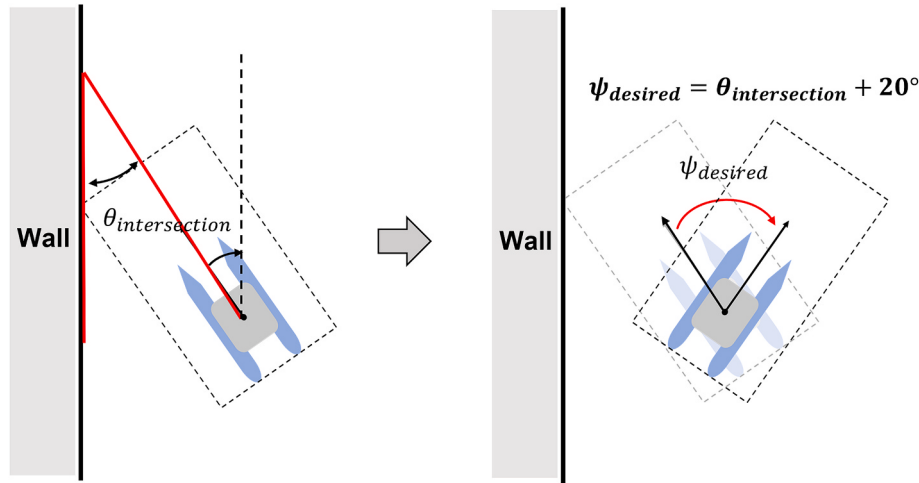


Fig. 8. Line OCAG

Fig. 12 shows the simulation results for Case 1 which the obstacle does not exist. **Fig. 12(a)** shows the trajectories of ASV, and the blue dots indicate the waypoints that ASV should follow. In **Fig. 12(a)**, it can be seen that circular curves are generated when moving to the next waypoint. The reason for these circular curves appears to be a delayed change of direction due to the effect of inertia, which was previously traveling at 1.1 m/s. In order to solve these delay problems, it can be improved through speed control such as deceleration considering the arrival time of the waypoint. **Fig. 12 (b)** shows the speed of the ASV, and it is confirmed that the steady-state speed can be reached by the speed controller after the speed decrease according to the direction change. **Fig. 12 (c)** shows the change of the heading angle of the ASV, and it is confirmed that the steering controller can follow the predefined path well with a slight overshoot after the change of direction. **Fig. 12 (d)** shows the change in the output of the ASV's thruster, and the difference in the output of the left and right thrusters occurs when the ASV needs to turn. At this time, the compatibility of the thruster is set in consideration of the specifications of the thruster manufacturer and is also reflected in the control command.

Finally, the simulation results of Case 1 confirm that the speed and steering controller of the ASV was properly designed. Also, it has been confirmed that the global path-following guidance well follows predefined waypoints like an autopilot.

Fig. 13 shows the simulation results for Case 2 in which a number of static obstacles exist. **Fig. 13(a)** shows the trajectory of the ASV moving from the bottom right to the destination on the top left, avoiding several

obstacles. In **Fig. 13 (a)**, the red box means the ship domain, and when an obstacle enters the region, it means that the ASV must move out so that the static obstacle can leave the region. At 2.5 s, the static obstacle is in the ship domain, so collision avoidance action is carried out by the predefined static OCAG as shown in **Fig. 7**. A not-smoothed curve is drawn in this step because an obstacle is detected in the ship domain and the ASV is moved out of the domain. When it was 5 s, it was confirmed that the first obstacle was stably avoided. At 10 s and 27 s, it was confirmed that the second and third obstacles were identified, respectively, and collision avoidance actions were taken. Also, no obstacles were detected between 15 and 27 s, so the ASV follows a predefined global path to the destination.

Fig. 13 (b) shows the speed of the ASV, and it was confirmed that the speed controller can stably reach the design speed after static obstacle collision avoidance. **Fig. 13 (c)** shows the change of the ASV's heading angle, and it was confirmed that obstacle collision avoidance is possible by the steering controller after detecting the obstacle. **Fig. 13 (d)** shows the change of the thruster output of the ASV, and it can be seen that the steering is performed through the difference in the output of the left and right thrusters when turning to avoid an obstacle collision. At this time, the steering controller is designed to have equal-sized outputs on the left and right thrusters for rotation.

Finally, simulation results of Case 2 confirm that the static obstacle avoidance guidance is effective in avoiding a number of static obstacles. And also, it is possible to return to the predefined global path after the obstacle is avoided.

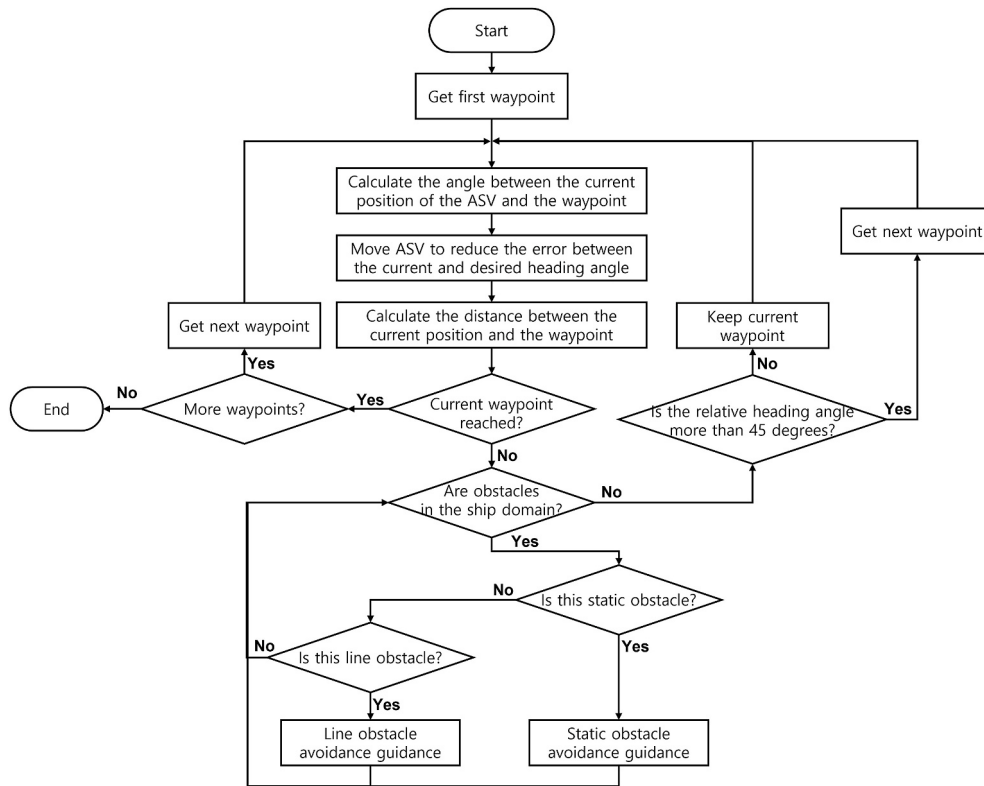


Fig. 9. Algorithm of collision avoidance system.

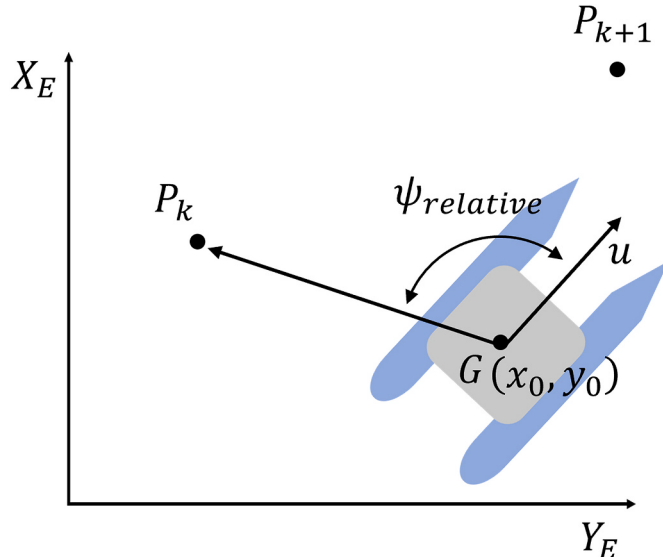


Fig. 10. Relative angle that can occur when completing collision avoidance.

Fig. 14 shows the simulation results for Case 3 in which static obstacles and wall obstacles exist evenly. Fig. 14 (a) shows the trajectory of the ASV moving from the bottom right to the destination on the top left, avoiding various types of obstacles. Also, in Fig. 14 (a), the red box means the ship domain. Also, no obstacles were detected until 8 s, so the ASV follows a predefined global route to the destination. After detecting static obstacles from 8 s to 13 s, it was confirmed that collision avoidance actions were taken according to the static obstacle avoidance guidance. The ship domain is set to 3 L in the forward direction, so the distance between the nearest wall and ASV is also 3 L. So between 16 and 18 s, it was confirmed that the wall was detected safely, and collision

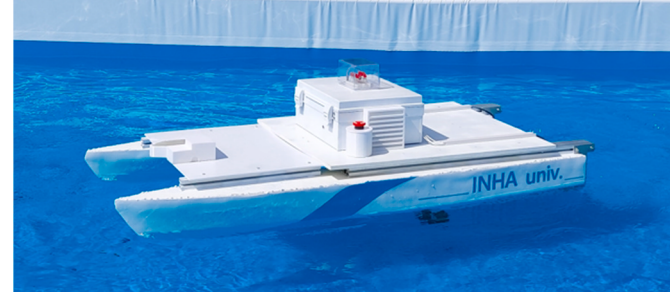


Fig. 11. Inha University Catamaran-type ASV

Table 1
Principal dimensions of the ASV.

| Parameter | Value |
|---------------------------------|---------|
| Length (L) | 1.445 m |
| Overall Breadth (B) | 0.767 m |
| Mono-hull Beam (b) | 0.187 m |
| Separation of centres (y_p) | 0.305 m |
| Draft (D) | 0.127 m |
| Displacement ($Disp.$) | 24.7 kg |

avoidance actions were taken according to the line obstacle avoidance guidance.

In Fig. 14 (b), it was confirmed that the speed controller can stably reach the design speed after obstacle collision avoidance. In Fig. 14 (c), it was confirmed that the steering controller can stably control the direction after detecting static and line obstacles. In Fig. 14 (d), it can be seen that when turning is necessary to avoid an obstacle collision, control is performed through the difference in the output of the left and right thrusters.

Table 2
Nondimensional hydrodynamic force coefficients used in the simulations.

| Parameter | Value |
|-----------|---------|
| X'_{vv} | -1.048 |
| Y'_{v} | -0.9901 |
| Y'_r | -0.2965 |
| Y'_r | 0.1899 |
| N_v | -0.4311 |
| N_r | -0.3164 |
| N_f' | -0.1425 |

Table 3
Initial conditions for simulations by case.

| ASV | Position of waypoints (WP) | | Position of obstacles (OBS, Line) |
|--------|----------------------------|----------------|--|
| | Position (m) | Velocity (m/s) | (m) |
| Case 1 | (0,35) | (0.77, 0.77) | WP1: (7,27)/ WP2: (6,15) WP3: (20,17)/ WP4: (5, 5) |
| Case 2 | (0,35) | (0.77, 0.77) | WP1: (20, 6) |
| Case 3 | (0,30) | (0.77, 0.77) | WP1: (20, 6) OBS1: (4, 30)/OBS2: (7,25) OBS3: (17, 10) OBS1: (7, 20) Line: ($x = 3y - 30, 0 \leq x \leq 15$) |

Finally, as a result of the simulation of Case 3, it was confirmed that the proposed static obstacle and line obstacle avoidance guidance are effective in performing collision avoidance by avoiding various types of obstacles in various encounter situations. Also, it was possible to return to the predefined global path after avoiding the obstacles.

4.3. Collision avoidance experiment results

Some experiments were performed by applying the proposed collision avoidance system in this study to an actual ASV. The ASV is equipped with a 2D LiDAR for the detection of obstacles and GPS and IMU sensors that can measure operating conditions. In addition, the proposed algorithm is installed on the main PC to give a collision-

avoidance command.

The experimental environment for verification is shown in Fig. 15. For experiments, we use the Google Maps Application Programming Interface (API) for remote control and monitoring stations to define the waypoint that the ASV should follow. There are two static obstacles in the generated global path, and in some cases, wall obstacles can be encountered.

The main situations in the collision avoidance experiments are largely divided into two categories: static obstacles and walls (representing line obstacles). For experiments, it is difficult to configure the same environment as simulation. Therefore, the ASV experiment was conducted in an environment where it is easy to directly verify the algorithm proposed in this paper. Fig. 16, Fig. 17, and Fig. 18 show the experimental results in the presence of static obstacles., and Fig. 19, Fig. 20, and Fig. 21 show the experimental results in the presence of a wall. The trajectory of the ASV has expressed in a plane coordinate system by converting longitude and latitude measured by GPS through Universal Transverse Mercator (UTM) projection. As shown in Figs. 16 and 19, the obstacle information detected with LiDAR was visualized in 3D through ROS RViz.

Case (i) Several static obstacles exist.

Case (ii) A wall obstacle exists.

As shown in Fig. 16, a collision-avoidance experiment was performed for Case 1 by placing static obstacles. Fig. 17 shows the trajectory of the ASV avoiding two static obstacles detected while the ASV is moving toward waypoint 1. When the ASV which was started from the top right encounters each obstacle, it can be seen that the collision avoidance actions were taken according to the predefined static obstacle avoidance guidance.

Fig. 18 shows the collision avoidance steering command by each guidance for obstacle avoidance. It was confirmed that the ASV turned right to avoid the first and second obstacle by static obstacle avoidance guidance between 3 and 16 s. In the process of returning to the predefined path after collision avoidance after 16 s, a new waypoint was selected because the relative angle between the ASV direction and the direction from the ASV to the current waypoint becomes more than 45° as shown in Fig. 10.

As shown in Fig. 19, a collision-avoidance experiment was performed for Case 2, considering the situation of moving toward the wall. There is

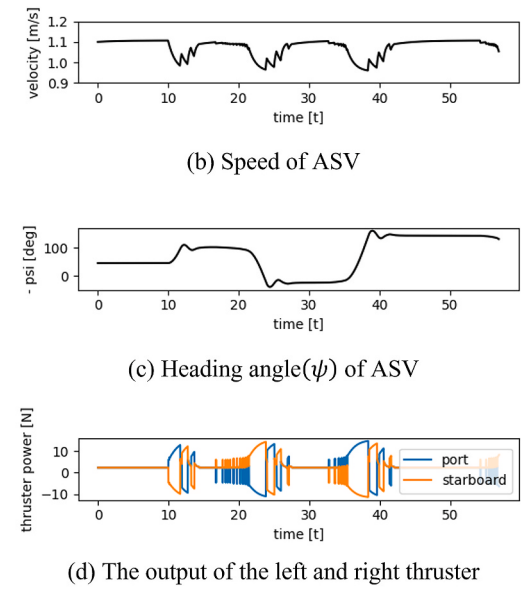
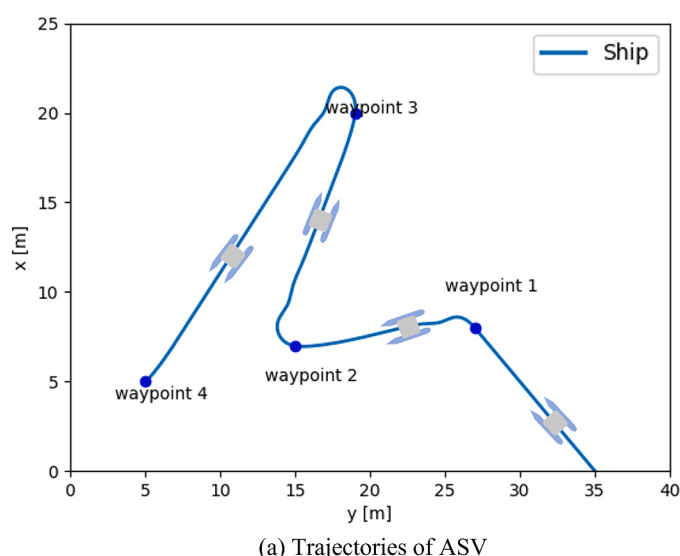


Fig. 12. Simulation results of Case 1.

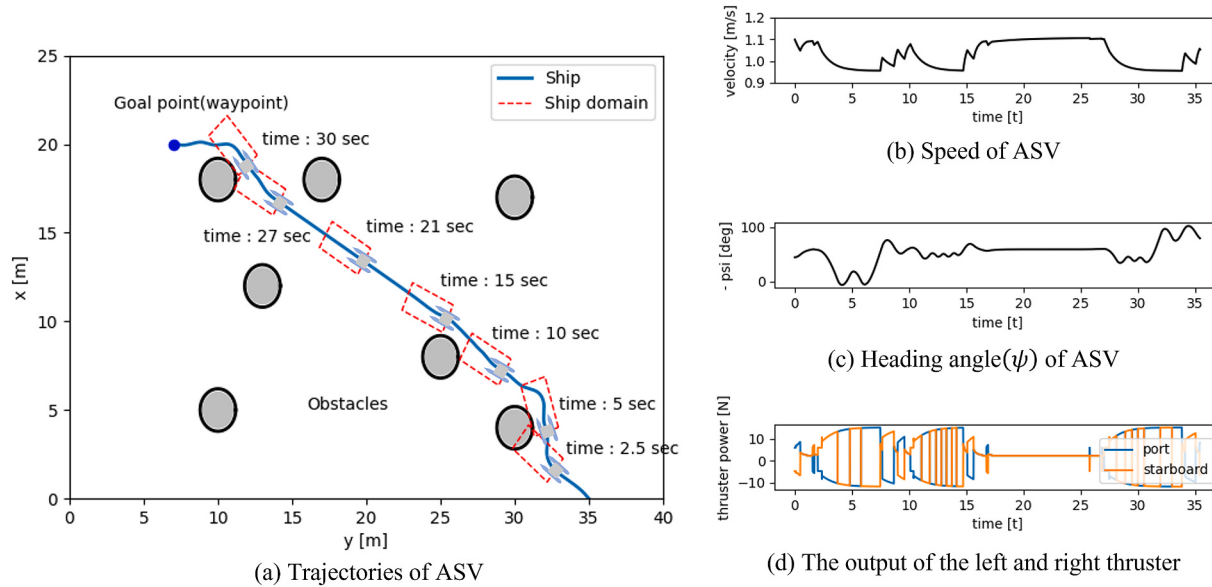


Fig. 13. Simulation results of Case 2.

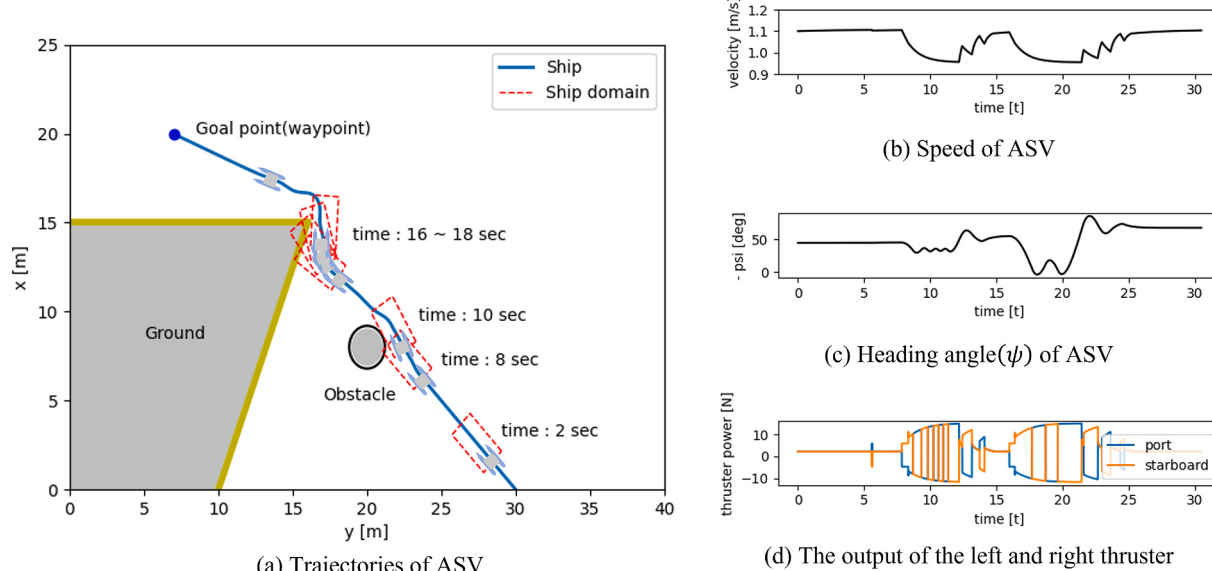


Fig. 14. Simulation results of Case 3.

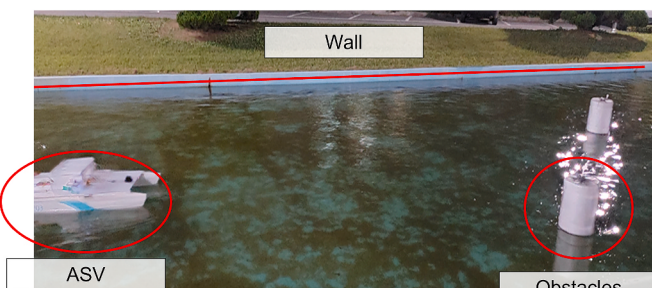


Fig. 15. Experiment environment.

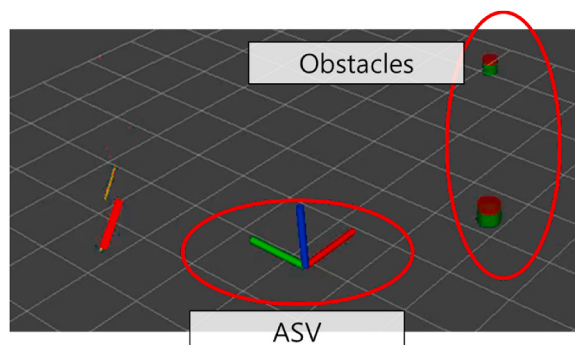


Fig. 16. Experiment conditions of Case 1.

a wall to the right of the ASV, and for a more intuitive observation, the ASV's final destination was set outside the wall so that it can continue to move towards the wall. Fig. 20 shows the trajectory of the ASV when it

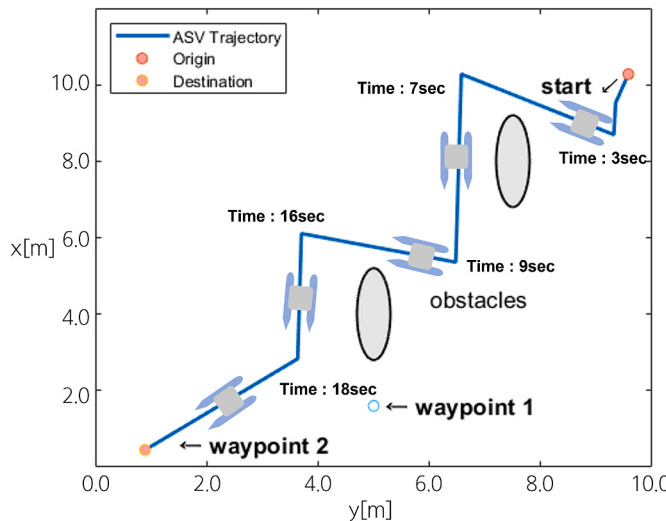


Fig. 17. ASV trajectory with fixed obstacles.

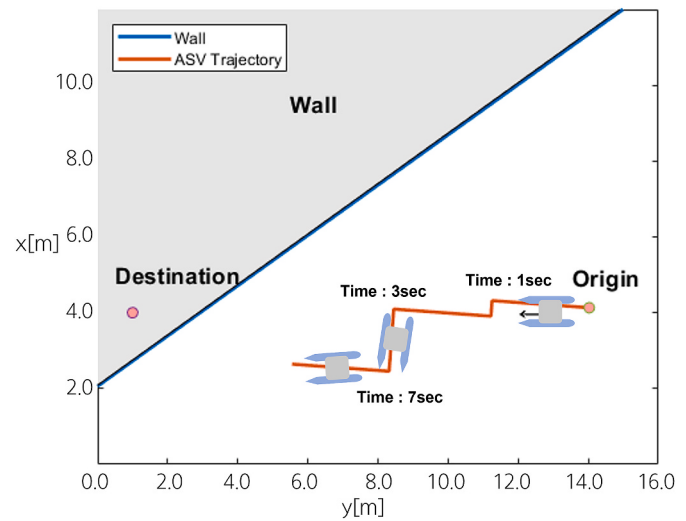


Fig. 20. ASV trajectory with wall obstacles.

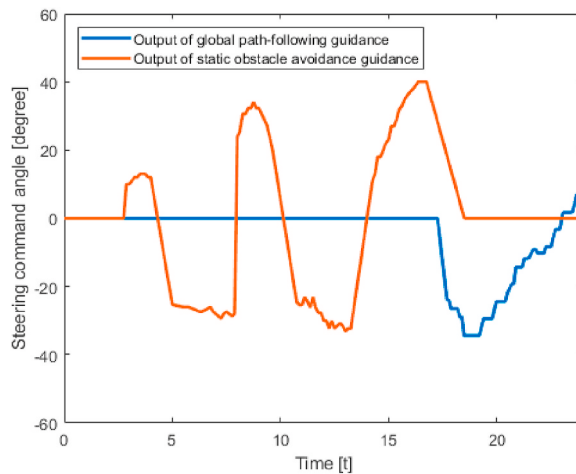


Fig. 18. Steering angle of the thruster with fixed obstacles.

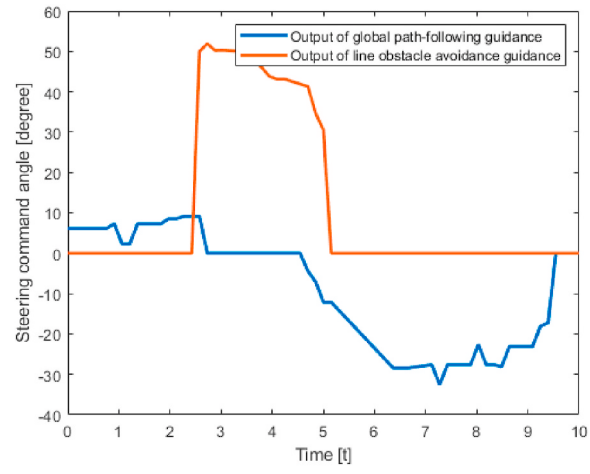


Fig. 21. Steering angle of thruster with wall obstacles.

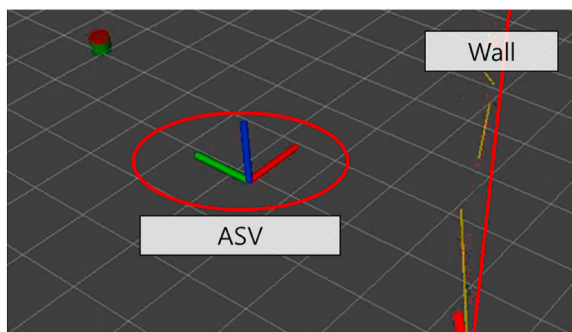


Fig. 19. Experiment conditions of Case 2.

encounters a wall such as a track obstacle. After encountering the wall, the ASV can be seen to reverse the direction to reduce the risk of collisions with the wall.

Fig. 21 shows the steering command angle for obstacle avoidance. Since no obstacles were detected in the ship domain until 2 s, ASV was heading to the destination according to the global path-following guidance. Between 3 and 5 s, the ASV detected the wall, added the angle between the ASV and the wall, and made additional compensation

according to the line obstacle avoidance guidance to give the steering command. In addition, the collision avoidance actions ended after 5 s, confirming that the ASV was heading to its original destination according to the global path-following guidance.

5. Conclusions

In this study, as a study on the collision avoidance system of ASV, we propose an obstacle collision avoidance system that can move to the destination while detecting and avoiding fixed obstacles with a 2D LiDAR sensor. Simulations and experiments were conducted to evaluate the performance of the proposed system, and the main conclusions are as follows.

1. The proposed obstacle collision avoidance system has been verified through simulation and experiment, and as a result, the proposed system detects and avoids obstacles and moves to the destination.
2. The speed controller and steering controller were designed to solve the underactuated ASV that requires speed and steering control at the same time through only thruster output control. Also, the proposed controller through simulation and experiment is suitable to follow the collision avoidance steering command.
3. When encountering static obstacles, the proposed collision avoidance guidance can make a safe path through direction correction and

- angle calculations where the obstacle leaves the ship domain of the ASV.
4. When encountering line obstacles (e.g. walls), the proposed collision avoidance guidance can reverse the direction by calculating the angle between the line and the ASV, and avoid the risk of collision through additional angle compensation for stable progress reversal.

In future studies, we will conduct research on advanced obstacle collision avoidance systems that satisfy the International Regulations for Preventing Collisions at Sea (COLREGs). The next goal is to avoid dynamic obstacles which were not considered in this work. Furthermore, since the GPS sensor used in this study has a low update frequency of 1 Hz, the resolution of position information is not high enough, so it will be supplemented in future studies.

CRediT authorship contribution statement

Ji-Soo Kim: Writing – original draft, Software, Methodology,

Appendix A. Determination of hydrodynamic force coefficients

(1) Virtual captive model tests with CFD (Static drift, pure sway, and pure yaw test)

Static drift, pure sway, and pure yaw simulations were performed using CFD to derive the hydrodynamic force coefficients to be used in the numerical method for maneuvering simulation of the ASV used in this study.

Static drift simulation

- We experimented by changing drift angle β from 0 deg to 12 deg at 3-deg intervals.

Pure sway simulation

- We experimented by changing nondimensional sway directional acceleration v' from 0.05 to 0.2 at 0.05 intervals.

Pure yaw simulation

- We conducted a simulation by changing nondimensional angular velocity r' from 0.1 to 0.6 at 0.1 intervals.

(2) Hydrodynamic force coefficients derived from CFD calculations

| Derivatives | CFD | Derivatives | CFD |
|-------------|---------|-------------|---------|
| Y'_v | -0.9101 | Y'_r | 0.1899 |
| N'_v | -0.3772 | N'_r | -0.3164 |
| Y'_v' | -0.1867 | N'_r' | -0.1425 |
| X'_{vv} | -1.048 | | |

References

- ABS, 2021. Guide for Autonomous and Remote Control Functions. American Bureau of Shipping.
- Ahn, D.S., Park, G.H., Choi, G.J., Jeon, S.Y., 2012. Researches on collision avoidance algorithms for autonomous driving system. Journal of the Korea Society For Power System Engineering 16, 84–90. <https://doi.org/10.9726/kspse.2012.16.1.084>.
- Campbell, S., Naeem, W., Irwin, G.W., 2012. A review on improving the autonomy of unmanned surface vehicles through intelligent collision avoidance manoeuvres. Annu. Rev. Control 36, 267–283. <https://doi.org/10.1016/j.arcontrol.2012.09.008>.
- Dong, Z., Wan, L., Li, Y., Liu, T., Zhang, G., 2015. Trajectory tracking control of underactuated USV based on modified backstepping approach. Int. J. Nav. Archit. Ocean Eng. 7, 817–832. <https://doi.org/10.1515/ijnaoe-2015-0058>.
- Fossen, T.I., 2002. Marine Control Systems—Guidance, Navigation, and Control of Ships, Rigs and Underwater Vehicles, Marine Cybernetics, Trondheim, Norway.
- Fujii, Y., Tanaka, K., 1971. Traffic capacity. J. Navig. 24, 543–552. <https://doi.org/10.1017/S037463300022384>.
- Han, J., Kim, D., Lee, M., Sunwoo, M., 2012. Enhanced road boundary and obstacle detection using a downward-looking LIDAR sensor. IEEE Trans. Veh. Technol. 61, 971–985. <https://doi.org/10.1109/TVT.2012.2182785>.
- Harmouche, M., Laghrouche, S., Chitour, Y., 2014. Global tracking for underactuated ships with bounded feedback controllers. Int. J. Control 87, 1–9. <https://doi.org/10.1080/00207179.2014.898188>.
- Islam, T., Islam, M.S., Shahid-Ul-Mahmud, Md, Hossam-E-Haider, M., 2017. Comparison of complementary and Kalman filter based data fusion for attitude heading reference system. In: AIP Conference Proceedings, 020002. <https://doi.org/10.1063/1.5018520>.
- Kim, J., Lim, D., Kim, D., 2020. Standardization status in maritime industry domain and ICT convergence trends. Electronics and Telecommunications Trends 35, 85–97.
- Klinger, W.B., Bertaska, I.R., von Ellenrieder, K.D., Dhanak, M.R., 2017. Control of an unmanned surface vehicle with uncertain displacement and drag. IEEE J. Ocean. Eng. 42, 458–476. <https://doi.org/10.1109/JOE.2016.2571158>.
- Liu, Z., Zhang, Y., Yu, X., Yuan, C., 2016. Unmanned surface vehicles: an overview of developments and challenges. Annu. Rev. Control 41, 71–93. <https://doi.org/10.1016/j.arcontrol.2016.04.018>.
- Premebida, C., Nunes, U., 2005. Segmentation and geometric primitives extraction from 2D laser range data for mobile Robot applications. 5rd National Festival of Robotics Scientific Meeting (ROBOTICA) 17–25.
- Song, H.W., Lee, K., Kim, D.H., 2019. Implementation of an obstacle avoidance system based on a low-cost lidar sensor for autonomous navigation of an unmanned ship. Trans. Korean Inst. Electr. Eng. 68, 480–488. <https://doi.org/10.5370/KIEE.2019.68.3.480>.

- Woo, J., Kim, N., 2020. Collision avoidance for an unmanned surface vehicle using deep reinforcement learning. *Ocean Eng.* 199, 107001 <https://doi.org/10.1016/j.oceaneng.2020.107001>.
- Yasukawa, H., Yoshimura, Y., 2015. Introduction of MMG standard method for ship maneuvering predictions. *J. Mar. Sci. Technol.* 20, 37–52. <https://doi.org/10.1007/s00773-014-0293-y>.
- Zhu, X., Zhao, T., Cheng, D., Zhou, Z., 2017. A three-step calibration method for tri-axial field sensors in a 3D magnetic digital compass. *Meas. Sci. Technol.* 28, 7. <https://doi.org/10.1088/1361-6501/aa58b9>.